

Broad-Band NMR with a High Spectral and Spatial Resolution

I. Serša¹ and S. Macura²

¹Department of Condensed Matter Physics, Jožef Stefan Institute, Ljubljana, Slovenia

²Department of Biochemistry and Molecular Biology, Mayo Graduate School, Mayo Clinic and Mayo Foundation, Rochester, Minnesota, USA

Received October 4, 2001

Abstract. Spatially selective excitation sequence CARVE (completely arbitrary regional volume excitation) excites signal from an arbitrarily shaped profile [Sersa I., Macura S.: *Magn. Reson. Med.* **37**, 920–931 (1997)] by an interleaved sequence of precalculated small tip angle radio-frequency pulses and gradient pulses. Here we propose a spatially selective observation method based on the CARVE principles which is insensitive to the relaxation and the off-resonance effects. The method, CARVE-D (CARVE detection), excites spins uniformly across the sample and across the spectrum but achieves spatial selectivity by weighted coaddition of the signals after the data acquisition. CARVE-D is suitable for spatially selective high-resolution nuclear magnetic resonance spectroscopy in chemically and geometrically complex systems. The method is analyzed theoretically, and demonstrated experimentally on model systems.

1 Introduction

Well-established techniques for volume localization of nuclear magnetic resonance (NMR) signal enable NMR observation only from simple geometries [1–8]. For excitation of complex profiles more sophisticated methods are used, most of which rely on simultaneous application of a shaped radio-frequency (RF) and gradient sequences [9–17]. The method we proposed for completely arbitrary regional volume excitation (CARVE) [13–15] consists of an interleaved train of short RF and gradient pulses. Design of all these sequences is based on the Fourier relationship between the excitation profile and the excitation sequence. The excitation sequence length depends on the complexity of the profile and the hardware properties. Profiles with complex geometry require more elementary steps for their accurate reproduction and, thus, require longer RF/gradient sequence. For long excitation sequence the signal relaxation during the sequence becomes significant which deteriorates excitation profile shape. Also, if resonance frequencies are spread, either due to chemical shift or local

field inhomogeneity, off-resonance components may distort resultant excitation profile. This makes the use of long RF/gradient sequences impossible for spatially selective spectroscopy. Many of these problems may be significantly reduced by volume selective observation techniques [18–21]. Here we propose a method for volume selective spectroscopy, CARVE-D (CARVE detection), on the basis of the volume selective observation derived from a CARVE sequence [22].

2 CARVE: Spatially Selective Excitation

An exact relationship between the excitation profile, $P(r, T)$, shaped RF pulse $B_1(t)$ and shaped gradient pulse $G(t)$ is given by [9, 14]

$$P(r, T) = \frac{M^+(r, T)}{i\gamma M_0(r)} = \int_0^T B_1(t) \exp[ik(t)r] dt, \quad k(t) = -\gamma \int_t^T G(t') dt', \quad (1)$$

where M^+ is a transverse and M_0 equilibrium magnetization density (magnetization per unit volume); $k(t)$ is continuous k-space trajectory. It is convenient to reformulate Eq. (1) in a discrete space [13–15, 17]. Then, a discrete profile, $P_N(r_n, T)$ is excited with a sequence of N RF pulses with complex tilt angles Θ_j , and N gradient pulses G_j

$$P_N(r_n, T) = \frac{M^+(r_n, T)}{iM_0(r_n)} = \sum_{l=1}^N \Theta_l \exp(ir_n k_l), \quad k_l = -\gamma \Delta t \sum_{j=l}^N G_j, \quad (2)$$

where Δt ($\Delta t = T/N$) is duration of a gradient pulse and k_l are elements of a discrete k-space walk.

Suppose that the ideal excitation profile $P(r)$ is defined by M^D discrete points which are equidistant in a D -dimensional cube with a side L . If the number of events in the excitation sequence is equal to the number of points in which the ideal profile is defined ($N = M^D$) then it is possible to excite the ideal profile, i.e., $P_N(r) = P(r)$. Short RF pulses are then equal to k-space coefficients of the ideal profile obtained by the inverse D -dimensional Fourier transform of the ideal profile [13]

$$\Theta_l = \frac{1}{M^D} \sum_{n=1}^{M^D} P(r_n) \exp(-ir_n k_l). \quad (3)$$

An ideal profile is usually defined on more points than the excitation sequence can have events ($M^D > N$). Thus, the excited profile is only an approximation of the ideal profile. A resemblance factor η , defined as a ratio of squares of the profile norms, quantifies the fidelity of the ideal profile approximation by the actual profile P_N [13, 14]

$$\eta = \frac{\|P_N\|^2}{\|P\|^2} = \frac{\sum_{l=1}^N |\Theta_l|^2}{\sum_{l=1}^{M^D} |\Theta_l|^2}. \quad (4)$$

One way of approximating the profile is illustrated in Fig. 1. The ideal profile ($D = 2$, $M^D = 65536$) is first transformed into k-space by an inverse two-dimensional (2-D) Fourier transformation Eq. (3), to obtain a complete set of 65536 coefficients Θ_l . Approximate profile P_N with $N = 250$ is obtained by the 2-D Fourier transformation, Eq. (2), of 250 k-space coefficients Θ_l with the highest amplitude (remaining $M^D - N$ coefficients are zeroed) yielding the approximation with the resemblance factor $\eta = 0.87$.

The excitation profile given by Eq. (2) corresponds to an ideal situation with magnetization on-resonance and negligible transverse relaxation. For magnetization set off-resonance by a frequency ω and with transverse relaxation time T_2 , Eq. (2) transforms to

$$P_{N,\omega,T_2}(r_n, N\Delta t) = \sum_{l=1}^N \Theta_l \exp[(N-l+1)\Delta t(-1/T_2 + i\omega)] \exp(ir_n k_l), \quad (5)$$

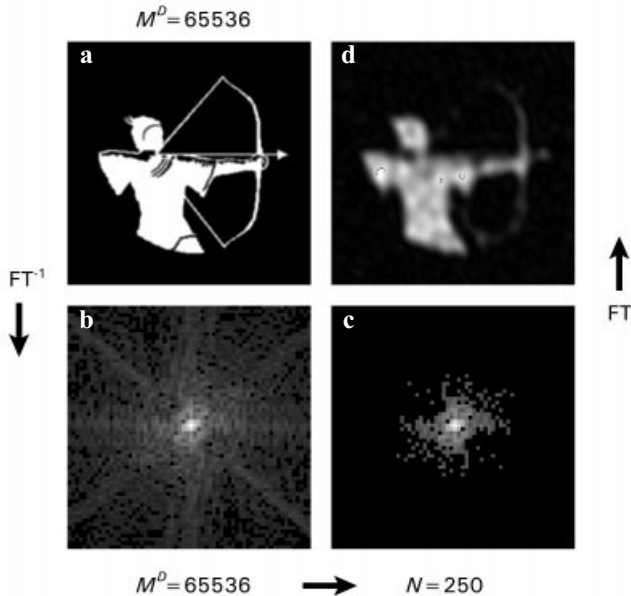


Fig. 1. Principle of a CARVE profile approximation. **a** Ideal excitation profile defined by one-bit image with a resolution 256 by 256, **b** a complete set of 65536 k-space coefficients calculated from the ideal profile by inverse Fourier transform, **c** 250 selected k-space coefficients with the highest amplitude and **d** approximated profile calculated from selected k-space coefficient by Fourier transform.

where $N\Delta t = T$ is total duration of the sequence. This equation can be viewed as a Fourier transformation of a product of two functions: \mathcal{O}_l and $\exp[(N - l + 1) \times \Delta t(-1/T_2 + i\omega)]$.

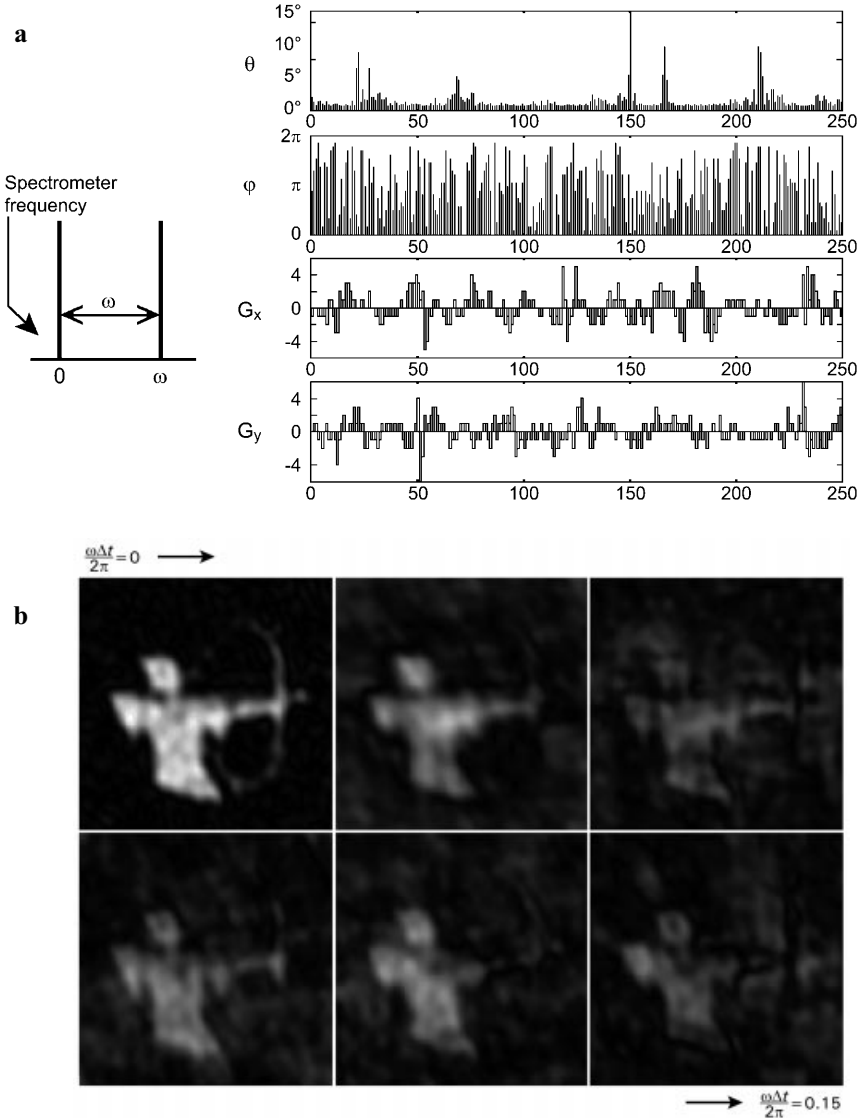


Fig. 2. Simulation of CARVE excitation profiles at different gradient pulse lengths for a sample with two spectral lines of the same amplitude. **a** CARVE spatially selective excitation sequence for excitation of the profile from Fig. 1d. The sequence consists of 250 excitation events calculated from a random k-space trajectory as described elsewhere [14]. **b** Excitation profiles simulated for linearly increasing gradient pulse lengths. The spectrometer frequency was set on the frequency of one spectral line.

The first function describes ideal relationship between the RF shape and the actual profile, and second takes into account the influence of relaxation and the resonance offset. Applying the convolution theorem to Eq. (5) one can conveniently express the actual profile $P_{N,\omega,T_2}(r_n, N\Delta t)$, over the on-resonance profile $P_N(r_n)$ and the point spread function $\text{PSF}_{N,\omega,T_2}(r_n, N\Delta t)$

$$P_{N,\omega,T_2}(r_n, N\Delta t) = P_N(r_n) \cdot \text{PSF}_{N,\omega,T_2}(r_n, N\Delta t), \quad (6)$$

where

$$\text{PSF}_{N,\omega,T_2}(r_n, N\Delta t) = \frac{1}{M^D} \sum_{l=1}^N \exp[(N-l+1)\Delta t(-1/T_2 + i\omega)] \exp(ir_n k_l). \quad (7)$$

The point spread function depends on the duration of the sequence, $N\Delta t$, and describes the blurring of individual profile pixels caused by the relaxation and the off-resonance effects. For a sample with more than one spectral line, i.e., when spins precess at different frequencies ω_j and relax with different relaxation times T_{2j} , each spectral line has its own point spread function. The excited profile is then a sum of excitation profiles of all spectral lines. Instead of the profile coaddition, the point spread functions can be summed yielding new PSF function for the whole spectrum

$$\text{PSF}_{N,\text{spectrum}}(r_n, N\Delta t) = \sum_{j=1}^J A_j \text{PSF}_{N,\omega_j,T_{2j}}(r_n, N\Delta t), \quad (8)$$

where A_j -s are amplitudes of J lines in the sample.

The influence of the off-resonance effect is demonstrated in Fig. 2. Shown profiles were calculated with Eq. (8) for $\omega = 810$ Hz and Δt linearly increasing from 0 up to 500 μs . Only the profile at $\Delta t = 0$ μs is identical to the on-resonance profile from Fig. 1d. All others have off-resonance artifacts that progressively increase with Δt .

3 CARVE-D: Spatially Selective Observation

Equations (2) and (3) which define relationship between the excitation profile and the RF pulse do not specify the way summation should be performed. In standard CARVE experiment the summation is performed in a single acquisition act after a series of RF and gradient pulses. Other possibility, which we call CARVE detection (CARVE-D) is to acquire data after each RF and gradient pulse pair and to coadd N separately acquired signals. This is illustrated in Fig. 3.

In the CARVE-D scheme, excitation is performed in a short time interval (single-event excitation: one RF pulse and one gradient pulse). Thus, there is no summation over time in the PSF and Eq. (7) simplifies to

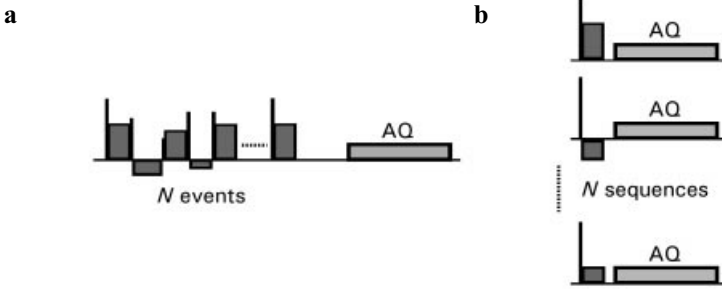


Fig. 3. Comparison of CARVE spatial selective excitation sequence **a**, and equivalent CARVE spatial selective observation sequences **b**. In CARVE-D N excitation events are distributed among N one-event excitation sequences for volume selective observation.

$$\begin{aligned} \text{PSF}_{N,\omega,T_2}^{\text{CARVE-D}}(r_n, \Delta t) &= \frac{1}{M^D} \exp[\Delta t(1/T_2 + i\omega)] \sum_{l=1}^N \exp(ir_n k_l) \\ &= \exp[\Delta t(-1/T_2 + i\omega)] \delta_N(r_n). \end{aligned} \quad (9)$$

Here δ_N is a Dirac delta function projected on a subset of N harmonics from which the observed profile is composed. A convolution between δ_N and the profile is therefore identical to the convolution between the regular delta function

$$\delta(r_n) = \frac{1}{M^D} \sum_{l=1}^{M^D} \exp(ir_n k_l)$$

and the profile. Then, in presence of the relaxation and the off-resonance effects CARVE-D excitation profile reduces to the convolution of PSF from Eq. (9) and the on-resonance profile

$$P_{N,\omega,T_2}^{\text{CARVE-D}}(r_n, \Delta t) = P_N(r_n) \cdot \text{PSF}_{N,\omega,T_2}^{\text{CARVE-D}}(r_n, \Delta t) = \exp[\Delta t(-1/T_2 + i\omega)] P_N(r_n). \quad (10)$$

In the last equation, in contrast to Eqs. (6) and (7), the off-resonance and the relaxation effects are independent of the number of experiments, N . They depend only on the duration of a single CARVE event, Δt . Most often this can be made sufficiently short that the off-resonance and the relaxation artefacts become negligibly small.

4 Relationship Between CARVE and CARVE-D

Equation (10) infers that in CARVE-D the off-resonance and the relaxation effects can be ignored for sufficiently short Δt . Then, even for chemically complex systems, CARVE-D can be analyzed by the on-resonance CARVE theory [14]. According to Eq. (2), resultant CARVE signal from the profile $P_N, S_{P_N}(t)$, is a sum of the signal components from individual volume elements, $M^+(r_n, N\Delta t, t)$

$$S_{P_N}(t) \equiv \sum_{n=1}^{M^D} M^+(r_n, N\Delta t, t) = \sum_{n=1}^{M^D} \sum_{l=1}^N iM_0(r_n, (N-l+1)\Delta t, t) \Theta_l \exp(ir_n k_l). \quad (11)$$

In CARVE the signal is recorded during the detection period, t , which begins after the excitation period $N\Delta t$, and the volume selection is achieved during the excitation sequence by superposition of the magnetization excited at different times $(l-1)\Delta t$ after the beginning of the sequence. The weighting is carried out by the RF pulses of different amplitudes and phases, Θ_l . In CARVE-D, magnetization components are excited in a series of N independent experiments each with the same excitation interval, Δt . Excitation pulses with the same amplitude and phase are used in all experiments and appropriate weights (proportional to the respective Θ_l -coefficient) are added in the post-processing. Then the signal from the profile P_N may be expressed as

$$S_{P_N}(t) = \sum_{n=1}^{M^D} \sum_{l=1}^N iM_0(r_n, \Delta t, t) \Theta_l \exp(ir_n k_l). \quad (12)$$

Equation (12) is almost the same as Eq. (11) with the only difference that the magnetization density M_0 , is the same in all experiments, i.e., M_0 is independent of the experiment index, l . Then the summations over N events (experiments) and over M^D spatial coordinates may be interchanged

$$S_{P_N}(t) = \sum_{l=1}^N \Theta_l \left[\sum_{n=1}^{M^D} iM_0(r_n, \Delta t, t) \exp(ir_n k_l) \right]. \quad (13)$$

The bracketed expression corresponds to a signal from the whole sample with a spatially dependent phase modulation imposed by a k-space vectors k_l . In other words, bracketed expression represents signal detected in the l -th CARVE-D experiment $S_l(t)$, and then

$$S_{P_N}(t) = \sum_{l=1}^N \Theta_l S_l(t). \quad (14)$$

Equation (14) gives prescription for the CARVE-D implementation. It shows that the volume selection can be achieved in the postprocessing by weighted averaging of signals recorded in a series of single-event excitation sequences with a constant tip angle, Fig. 3b. The excitation bandwidth depends on the properties of the constant tip angle pulse in complete analogy to 1-D spectroscopy. For sufficiently short interval Δt , Eq. (14) holds for any sample irrespectively of the number and distribution of spectral lines.

5 Methods and Results

Experiments were performed on a 300 MHz Bruker Avance spectrometer equipped with microimaging accessories.

5.1 Homogeneous Sample

We tested the feasibility of CARVE-D on a homogeneous sample with two spectral lines, a 15 mm tube filled with CuSO_4 -doped mixture of water and acetone. The target profile was an image of an archer from Fig. 1a. A complete set of Θ_i coefficients was calculated with Eq. (3) (2-D inverse Fourier transform of the ideal profile) and 1000 coefficients with the highest amplitude were selected to define the profile. To visualize the observation profile, modified gradient-echo imaging sequence was used as described previously [22]. In total

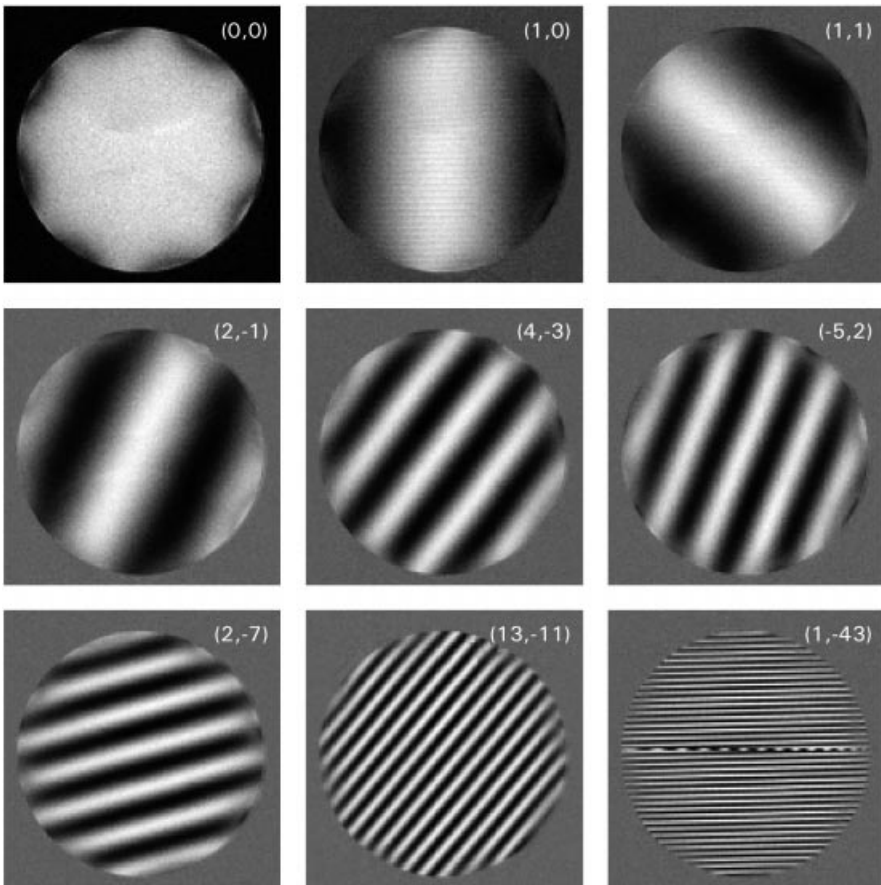


Fig. 4. Few representative base images (out of 1000) that were used for visualization of the observation profile from Fig. 1a. Images of a water-acetone-filled tube in axial slices are presented with their real component of the signal. Different direction and frequency of spatial oscillations in signal intensity in the images are due to different k-space encoding of the images. Coordinates of k-space vectors (in units of $2\pi/L$ where L is field of view) to which images correspond are written in brackets in the upper right corner of each image. Imaging parameters were: field of view, 15 mm; slice thickness, 2 mm; repetition rate, 30 ms and matrix size, 128 by 128 points.

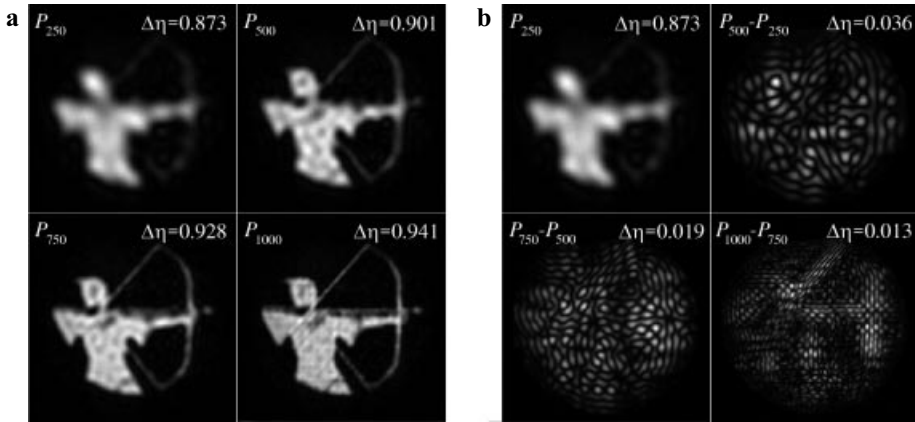


Fig. 5. Visualized CARVE-D profiles. **a** Total profiles with increasing number of coefficients. **b** Partial observation profiles composed from base images (Fig. 4) that are ordered by increasing modulation vector (k) amplitude. The ideal observation profile is a profile in Fig. 1a.

1000 different gradient-echo imaging sequences were used, one for each k -space point. All 1000 images have identical magnitude but different phases, Fig. 4. Whereas individual base images are not spatially selective, their weighted sum is. This is demonstrated in Fig. 5 with CARVE-D profiles obtained by weighted

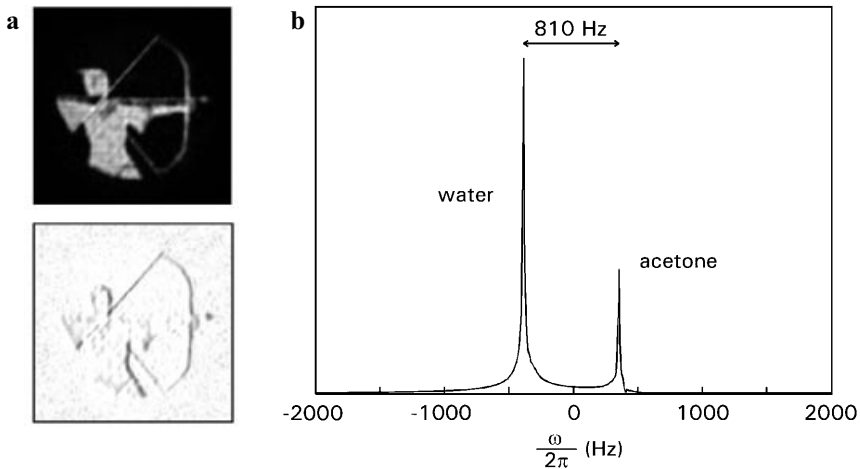


Fig. 6. CARVE-D in a homogeneous sample. **a** Measured observation profile (top) and its difference to the theoretical profile (bottom) in a water-acetone-filled tube. The profile, with the best resemblance to its ideal profile in Fig. 1a, is a weighted sum of $N = 1000$ base images. **b** A spectrum from the observed sample region: size, 8192 points; spectral width, 50 kHz and repetition time, 1000 ms. The spectrum in Fig. 6b which calculated from the final FID signal by a regular 1-D Fourier transform preserved its spectral resolution regardless of its complex spatial observation profile.

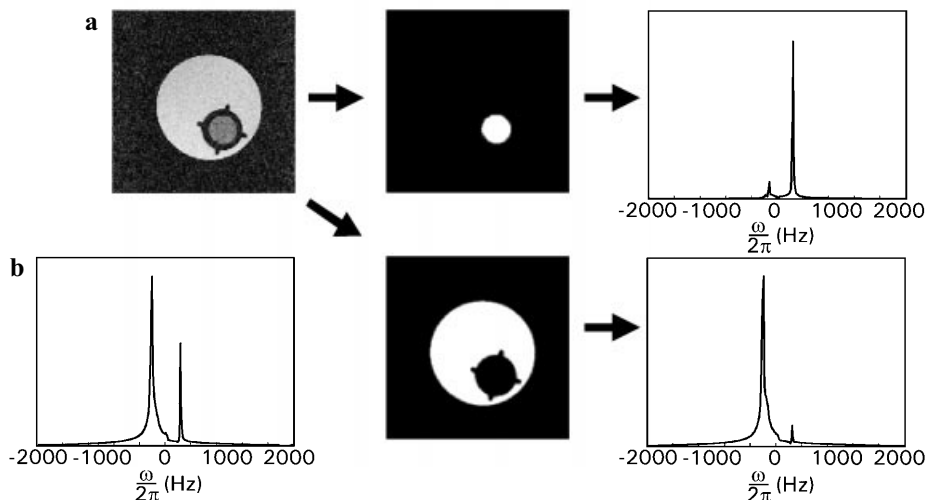


Fig. 7. CARVE-D in a heterogeneous sample: **a** A sample consists of outer water-filled tube and inner acetone-filled tube. **b** Spectrum from the sample acquired by nonselective excitation. From the image of the sample (field of view, 25 mm; slice thickness, 2 mm) two observation profiles (masks) were designed: **c** for observation of the acetone compartment and **d** for observation of the water compartment. Corresponding spectra from these two compartments: **e** acetone spectrum and **f** water spectrum. Both were acquired with the spatially selective observation with $N = 250$ events. Spectra were acquired with 1024 data points, 5 kHz spectral width and 1 s repetition rate.

summation of base images. Figure 5a shows CARVE-D profiles generated with an increasing number of base images. Obviously the resolution of the profile increases with the number of base images. This is illustrated in Fig. 5b which shows a profile with $N = 250$ and a differences between the successive profiles from Fig 5a. Higher-index terms have higher-frequency components which sharpen the profile.

Figure 6 demonstrates the agreement between the theoretical and experimental profiles with $N = 1000$. The difference between the two profiles is negligible and shows only at the edges of the profile in the readout direction. These are most probably present due to a small chemical shift artifact. Figure 6b shows the spectrum obtained with a CARVE-D scheme (Fig. 3b) with $N = 1000$ and the same set of k-space encoding gradients as used for the profile visualization. Acquired 1000 free induction decay (FID) signals were co-added according to Eq. (12) to yield FID from the profile. The spectrum is obtained by 1-D Fourier transformation of the resulting FID.

5.2 Heterogeneous Sample

To test performance of CARVE-D for assessing spectral information from different compartments a test sample with two tubes was used, Fig 7a. A 4 mm

diameter tube filled with acetone was placed into the outer 15 mm diameter tube filled with water. Two excitation profiles were generated from a regular MR image of the sample in axial cross-section, Fig. 7a. The first profile, Fig. 7c, corresponds to the inner tube and the second, Fig. 7d, to the water compartment. Upon the profile selection the k-space coefficients were calculated and 250 coefficients with the highest amplitude were used for CARVE-D experiment. The resemblance factor of the profile, Eq. (4), was 0.90. The final spectra from selected profiles were obtained from the weighted sum of the individually acquired signals, Eq. (12). In the spectrum from the inner tube, Fig. 7e, the acetone line is predominant and in the outer tube, Fig. 7f, major is the water line which correspond to their respective chemical composition.

6 Discussion

The CARVE method is designed to excite signal from arbitrarily shaped volume. The volume is defined from a prerecorded pilot image of the studied object. The excited volume does not need to be continuous, i.e., the selected excitation profile may comprise several separate regions. For example, some brain lesions (Alzheimer plaques, neuron demyelination etc.) are scattered all over the brain and recording spectra from them by traditional volume selective methods is virtually impossible. The CARVE method is capable of exciting a signal simultaneously from all the regions identified in the pilot image. Once the regions are identified, appropriate CARVE sequence with desired degree of approximation can easily be designed and executed, as depicted in Fig. 1. Since a degree of approximation of the ideal profile depends on the shape of the profile and the number of Θ -coefficients used, the CARVE sequence usually comprises several hundreds to several thousands RF/gradient pulse pairs. Because of the finite width of the gradient pulses the total execution time of the CARVE sequence may range from few milliseconds to few hundreds milliseconds. In CARVE, like in other constant frequency excitation sequences, the excitation bandwidth is inversely proportional to the excitation sequence length. That means that high-definition CARVE sequence necessarily is a narrow band frequency excitation. This property of the sequence may be beneficial if both, frequency and space selectivity are desired. For example, one can monitor concentration of only one selected component within several complex shaped compartments.

However, a broad-band spatially selective excitation is more desirable. This can be easily achieved by suitable modification of the CARVE sequence. The CARVE excitation can be viewed as a Fourier series expansion of the desired profile in k-space, i.e., excitation profile is built by summing up its respective Fourier coefficients in k-space. The coefficients are sampled by short RF pulses (with appropriate tilt angles and phases) executed at corresponding k-space points. The sequence duration is determined by the rate by which k-space points can be visited which, in turn, depends exclusively on the properties of the gradient unit. Thus, excitation bandwidth of the CARVE sequence is artificially controlled by

the limitations of the gradient units. Since individual RF pulses are short enough to provide uniform excitation across the whole spectrum, it is important to consider what happens to the signal from the off-resonance spins. Off-resonance spins are stimulated by each short RF pulse but since their time evolution is unrelated to the phases of the RF pulses their trajectories are unpredictable. This manifests either as the profile blurring or as a rise of the noise floor in regions outside the profile, Fig. 2. Undesirable effects of the off-resonance that in the profile image show as an increase of the noise floor, in the corresponding spatially selective 1-D spectrum propagate as an amplitude modulation of off-resonance spectral lines irrespectively of whether the lines are inside or outside the profile. These effects can be easily removed if the visitation of one k-space point is temporally detached from the visitation of other points, i.e., if individual k-space points are visited in separate signal acquisitions. This means that, instead in one N -events sequence, Fig. 3a, desired profile is excited by signal superposition from N one-event sequences, Fig. 3.

Apparently, the increase of the band width has to be paid by the N -fold increase in the number of experiments. However, for heteronuclei or when the profile represents a small fraction of the total sample volume, the signal averaging must be performed anyway. Then, the CARVE-D method can be merged into the signal averaging resulting in just a moderate increase of the total experimental time: $TT_{\text{CARVE-D}}/TT_{\text{CARVE}} = N/N_A$, where N_A is the number of averages. Even in the worst case, with the N -fold increase of the experimental time CARVE-D is M^D/N times faster than the full volume imaging spectroscopy.

In terms of spatial selectivity CARVE and CARVE-D are identical, as expressed by Eqs. (11) to (14). Equation (14) shows that broad band signal from desired profile can be obtained by coaddition of N signals acquired by the single-event sequence. To depict the profile generation from individual signals, experiments were performed as a series of 2-D images. Figure 4 shows few such images in phase-sensitive mode with different k_l components, (k_x, k_y) . Image with $k_x = k_y = 0$ corresponds to a standard spin density image, which for a tube filled with the water/acetone mixture should have uniform intensity across the whole circular cross section. Small deviation at the edges is due to the B_1 field inhomogeneity of the bird cage resonator. All other images are phase modulated along the x - and y -direction by the respective components of the k-space vectors. A sum of phase modulated images weighted according to Eq. (14) generates desired profile, as shown in Fig 5. It is obvious that for sufficiently large number of experiments, the experimental profile can be made to approximate the ideal profile with the desired resemblance factor.

High fidelity of CARVE-D can be evaluated from Fig. 6a where the experimental profile (top) with $N = 1000$ is compared with the difference between the experimental (water acetone mixture) and the theoretical on-resonance profile. A small difference in the readout direction is most likely an artefact of the imaging method rather than the CARVE-D. Namely, water and acetone lines (at 7 T) are separated for 810 Hz which, in the image recorded with 50 kHz spectral width in a 128 by 128 matrix, shows as a splitting of roughly two pixel apart.

A broad-band character of the CARVE-D method is demonstrated in Fig. 6b which shows the spectrum calculated from the profile in Fig. 6a. The spectrum corresponds to the chemical composition of the sample (doped water/acetone mixture) in the same ratio as obtained in a standard 1-D spectrum (not shown).

Principal aim of the CARVE-D method is a rapid recording of the volume-selective high-resolution spectra with high spatial and spectral resolution, which is demonstrated in Fig. 7. The test sample, Fig. 7a, consisting of two compartments filled with water (outer) and acetone (inner) was used to demonstrate spatial selectivity. The standard 1-D spectrum contains both, the water and the acetone line, Fig. 7b. However, CARVE-D spectra obtained from the profiles corresponding to the original compartments, Fig. 7c, d, faithfully reproduce their respective chemical composition. The spectrum from the inner compartment, Fig. 7e, contains a strong acetone line and from the outer the water line. Presence of a small residual signal from the unobserved compartment merits a comment. It is most likely caused by partial resonance saturation due to a high repetition rate. This is corroborated by evidently much better suppression of water line than of the acetone line. The acetone methyl group relaxes much slower and is easier to saturate than water. A suppression factor of almost 20 for water line (the water/acetone ratio in 1-D vs. the ratio in the acetone compartment) verifies the great spatial selectivity of the CARVE-D method.

7 Conclusions

CARVE-D has numerous advantages over CARVE. It enables signal acquisition from complex observation profiles and preserves all properties of high resolution spectra. The method is insensitive to signal relaxation and off-resonances. Besides, it does not require any special gradient hardware and can be therefore implemented on practically any imaging system. Longer experiment times that are inevitable at observation of signals from complex profiles may be successfully merged into signal averaging. In this paper, only few simple applications of CARVE spatially selective observation were presented to demonstrate its feasibility. However, many more applications ranging from medical applications in clinical environment where the targeted profiles may be human organs to the applications in technology where one would be interested in examining material properties in a high-field microimaging system can be found.

References

1. Mueller S., Aue W.P., Seelig J.: *J. Magn. Reson.* **65**, 332–338 (1985)
2. Aue W.P., Muller S., Cross T., Seelig J.: *J. Magn. Reson.* **56**, 350–354, (1984)
3. Frahm J., Haenicke W.: *J. Magn. Reson.* **60**, 320–332 (1984)
4. Doddrell D., Bulsing J., Galloway G., Brooks W., Field J., Irving M., Baddeley H.: *J. Magn. Reson.* **70**, 319–326 (1986)
5. Doddrell D.M., Brooks W.M., Bulsing J.M., Field J., Irving M.G., Baddeley H.: *J. Magn. Reson.* **68**, 367–372 (1986)

6. Connelly A., Lohman J.: *J. Magn. Reson.* **66**, 283–294 (1986)
7. Connelly A., Counsell C., Lohman J.: *J. Magn. Reson.* **78**, 519–525 (1988)
8. Frahm J., Hänicke W.: *J. Magn. Reson.* **60**, 320 (1986)
9. Pauly J., Nishimura D., Macovski A.: *J. Magn. Reson.* **81**, 43–56 (1989)
10. Pauly J., Nishimura D., Macovski A.: *J. Magn. Reson.* **82**, 571–587 (1989)
11. Meyer C.H., Pauly J.M., Macovski A., Nishimura D.G.: *Magn. Reson. Med.* **15**, 287–304 (1990)
12. Spielman D., Pauly J., Macovski A., Enzmann D.: *Magn. Reson. Med.* **19**, 67–84 (1991)
13. Sersa I., Macura S.: *J. Magn. Reson. B* **111**, 186–188 (1996)
14. Sersa I., Macura S.: *Magn. Reson. Med.* **37**, 920–931 (1997)
15. Sersa I., Macura S.: *J. Imag. Sci. Tech.* **10**, 225–241 (1999)
16. Morrell G., Macovski A.: *Magn. Reson. Med.* **37**, 378–386 (1997)
17. Serša I., Macura S.: *J. Magn. Reson.* **135**, 466–477 (1998)
18. Morris G.A., Freeman R.: *J. Magn. Reson.* **29**, 433–462 (1978)
19. Mareci T.H.: *J. Magn. Reson.* **57**, 157–163 (1984)
20. Brooker H.R., Mareci T.H., Mao J.: *Magn. Reson. Med.* **5**, 417–433 (1987)
21. Hu X., Levin D.N., Lauterbur P.C., Spraggins T.: *Magn. Reson. Med.* **8**, 314–322 (1988)
22. Serša I., Macura S.: *J. Magn. Reson.* **143**, 208–212 (2000)
23. Metropolis N., Rosenbluth A.W., Rosenbluth M.N., Teller A.H., Teller E.: *J. Chem. Phys.* **21**, 1087–1092 (1953)
24. Scheffler K., Henning J.: *Magn. Reson. Med.* **35**, 569–576 (1996)

Authors' address: Igor Serša, Jožef Stefan Institute, Jamova 39, 1000 Ljubljana, Slovenia